Wave Digital Modeling and Implementation of Nonlinear Audio Circuits with Nullors

Wave Digital Modeling and Implementation of Nonlinear Audio Circuits with Nullors

Riccardo Giampiccolo, *Graduate Student Member, IEEE*, Mauro G. de Bari,
Alberto Bernardini, *Member, IEEE*, Augusto Sarti, *Senior Member, IEEE*

Abstract—The nullor is a theoretical two-port element suitable to model several multi-port devices common in audio circuitry, such as ideal operational amplifiers, operational transconductance amplifiers, and transistors operating in linear regime. In this manuscript, we present an approach for the Wave Digital (WD) modeling and implementation of circuits with multiple nullors. In particular, we propose an approach to compute scattering matrices of WD topological junctions absorbing nullors that is less computationally demanding than the techniques available in the literature on WD Filters. We show that the proposed approach turns out to be particularly useful when simulating nonlinear circuits through the Scattering Iterative Method (SIM), a WD fixed-point method recently developed for the solution of circuits with multiple nonlinearities, because it requires a frequent update of the scattering matrices. We also provide a novel convergence analysis of SIM applied to WD structures composed of multiple one-port nonlinear elements and a topological junction absorbing nullors. In order to verify the effectiveness of the proposed methodology, we discuss some WD implementations of analog audio circuits with multiple diodes and opamps, including a precision half-wave rectifier and a wave folder circuit.

Index Terms—Wave Digital Filters, nonreciprocal connection networks, nullors, nonlinear audio circuits.

I. INTRODUCTION

VIRTUAL Analog (VA) modeling is achieving resounding success in the audio market, being at the basis of several digital audio plug-ins. VA modeling refers to that class of digital audio algorithms specifically designed to emulate analog audio equipment [1]. Many musicians and sound engineers, in fact, relish VA products for being cheaper and less bulky with respect to their analog counterparts. The peculiar sound qualities of analog audio circuits are especially due to their nonlinearities [2]. For instance, several audio compressors, saturators, wave folders, or wave shapers exploit diode chains to modify and increase the harmonic content of audio signals. In the literature, VA modeling is addressed employing two main methodologies: *black-box approaches* that infer a reference circuit model starting from pairs of input/output data, e.g., using neural networks [3] or descriptions based on the Volterra series [4]; *white-box approaches* that emulate the reference circuit by simulating the corresponding system of ordinary differential equations, e.g., using the State-space method [5], the Port-Hamiltonian method [6], or Wave Digital Filters (WDFs) [7]. White-box techniques are generally more accurate

R. Giampiccolo, M. G. de Bari, A. Bernardini, and A. Sarti are with the Dipartimento di Elettronica, Informazione e Bioingegneria (DEIB), Politecnico di Milano, Piazza L. Da Vinci 32, 20133 Milano, Italy. Corresponding author: Riccardo Giampiccolo (email: riccardo.giampiccolo@polimi.it).

than black-box methods though they might be characterized by a high computational cost, especially when dealing with circuits with multiple nonlinearities. However, since modern audio interfaces are equipped with banks of Digital Signal Processors (DSPs) and/or Field-Programmable Gate Arrays (FPGAs) to which the processing of digital effects in Digital Audio Workstations (DAWs) can be offloaded, there will be the possibility of implementing increasingly computationally demanding VA algorithms in the near future.

Among white-box techniques, WDF methods are proving to be very promising tools. First introduced by A. Fettweis in the '70s for the design of digital filters based on the discretization of reference passive circuits [7], sharing some common features of Transmission-Line Modeling techniques [8], WDF theory is based on a port-wise description of a reference circuit, where port currents and port voltages (the so-called Kirchhoff variables) are substituted with linear combinations of incident and reflected waves with the introduction of a free parameter per port called *port resistance*. WDFs are highly modular, since they allow us to model circuit elements and topological connection networks in a separate fashion. The reference circuit is represented in the WD domain as an interconnection of one-port and multi-port WD blocks, each characterized by a scattering relation that expresses the reflected waves as functions of the incident waves. By properly choosing port resistances and making use of stable discretization methods (e.g., trapezoidal rule, Backward Euler, etc.) [9], circuits containing linear elements and up to one nonlinear element (characterized by an explicit WD scattering relation) can be implemented in the WD domain in a fully explicit fashion, i.e., removing all the implicit equations, called *delay-free-loops* (DFLs) in the WDF literature [7]. This is done by setting the free parameters of WD structures in such a way that certain ports of circuit elements or WD junctions are made reflection-free: in WDF theory such a process is called *adaptation* [7], [10]. However, when the reference circuit is characterized by multiple nonlinear elements, the adaptation process is not sufficient to eliminate all the DFLs, and iterative procedures must be used to solve the reference circuit. Several iterative Wave Digital (WD) methods to solve circuits with multiple nonlinearities are discussed in the literature [11]–[14]. Amongst others, the Scattering Iterative Method (SIM) [13], [15] is an efficient fixed-point method that is paving the way towards the real-time implementation of several circuits containing multiple nonlinear elements [9], [16]. Moreover, lots of SIM operations are embarrassingly parallelizable, leading the way towards the parallel digital implementation of large

nonlinear audio circuits.

The modeling of *connection networks* as multi-port scattering junctions characterized by scattering matrices is an essential aspect of the WD implementation of analog circuits. It has been shown in [16] that the formation of scattering matrices of junctions is the bottleneck of the SIM algorithm, therefore, the development of efficient strategies for their computation is in order. Connection networks can be classified according to their properties, such as reciprocity and losslessness [17], [18]. A peculiar class is the one of *lossless reciprocal connection networks* [18], [19], that include pure topological junctions, i.e., interconnections of wires and junctions embedding ideal transformers. Connection networks embedding linear nonreciprocal multi-ports, such as gyrators, controlled sources, or *nullors* [17], are, instead, often nonreciprocal, and can be either active, lossy, or lossless. A general approach for the WD realization of arbitrary (reciprocal, nonreciprocal, lossless, or nonlossless) connection networks is presented in [17] and is based on the Modified Nodal Analysis (MNA) framework. Another approach solely applicable to lossless reciprocal connection networks, which is less general though more efficient than [17], is presented in [18], [19]. Linear multi-ports are often embedded in the WD scattering junctions because they would otherwise cause DFLs, as extensively discussed in [17], [20]. In the recent publication [20], however, it has been shown that, by adopting a vector definition of wave variables for modeling two-port linear elements in the WD domain, a large class of two-ports can be adapted (i.e., the dependence of the pair of reflected waves on the pair of incident waves is removed) thus eliminating the DFLs that would otherwise arise when using scalar definitions of wave variables. Not only the approach in [20] increases the modularity of WDFs, but it also leads to more efficient WD implementations of a large class of circuits containing linear multi-ports [20]. As a further remarkable result, it has been shown in [20] that using vector waves, unlike the case of scalar waves, it is possible to derive a wave-based description of the nullor as a separate two-port. Unfortunately, even using vector waves the nullor cannot be adapted [20]; hence, the MNA-based approach presented in [17] that embeds nullors into topological junctions is still preferable when the reference circuit contains more than one nullor because DFLs are avoided. Nevertheless, according to the approach in [17], each nullor adds a row and a column to the MNA matrix, and thus the cost of its inversion and, consequently, the cost to compute the scattering junction matrix can become significantly high.

However, circuit models containing multiple nullors are useful in VA modeling [21], [22]. In fact, although nullors are theoretical two-port elements with no physical counterpart, they can be employed to model numerous other multi-ports, such as ideal transistors [21], [23], vacuum tubes, operational amplifiers (opamps) [17], [20], [22], and operational transconductance amplifiers (OTAs) [21] operating in linear regime, usually simplifying the system of equations that describes the reference circuit [24]–[26]. Moreover, the nullor also proved to be the essential circuit element in the context of inverse VA modeling [27].

In this manuscript, we propose a novel approach that is less

computationally demanding than the one presented in [17] for the implementation of WD junctions absorbing nullors. The proposed approach is an extension of the efficient method discussed in [18], [19] solely applicable to lossless reciprocal connection networks. The proposed method relies on the fact that a nonreciprocal network containing nullors can be represented using a pair of complementary reciprocal networks. We show that the speed-up provided by the proposed method is particularly useful when implementing circuits characterized by multiple nonlinearities with the SIM algorithm. Indeed, as extensively discussed in [16], the update of the scattering junction matrix is the most computationally demanding operation of SIM. We also provide a novel convergence analysis of the SIM algorithm when applied to WD structures with multiple nonlinear one-ports and a single nonreciprocal junction embedding nullors. In fact, the studies on SIM convergence present in the literature are restricted to WD structures with lossless reciprocal junctions [9], [13].

The manuscript is organized as follows. Section II provides background knowledge on WDFs, in particular on the modeling of linear and nonlinear one-ports. After recalling the nullor constitutive equation, Section III introduces the novel method for the WD realization of connection networks embedding nullors, and it discusses its advantages in terms of computational cost with respect to the MNA-based method presented in [17]. Section IV gives an overview on the SIM algorithm, and it provides a novel convergence analysis of SIM applied to WD structures characterized by nonreciprocal scattering junctions absorbing nullors. Two examples of application of the proposed approach are reported in Section V. Section VI concludes this manuscript.

II. MODELING ONE-PORTS IN THE WD DOMAIN

The design process of Wave Digital Filters (WDFs) [7] starts from a port-wise description of the reference analog circuit, in which elements and connection networks can be independently handled. Each port of a WD block is characterized by an *incident wave* a and a *reflected wave* b, defined as linear combinations of the port voltage v and the port current i. Different definitions of wave variables (which lead to different benefits) are available in the literature [7], [10], [17], [18], [28]. In [17], [18], the following generalized parametric definition of waves has been discussed

$$a = Z^{\rho-1}v + Z^\rho i, \qquad b = Z^{\rho-1}v - Z^\rho i, \qquad (1)$$

where $Z \neq 0$ is a free parameter called *port resistance* and $\rho \in \mathbb{R}$ determines the wave type. It is also useful to express the inverse mapping of (1), which is

$$v = Z^{1-\rho}\frac{(a+b)}{2}, \qquad i = Z^{-\rho}\frac{(a-b)}{2}. \qquad (2)$$

Current, power, and voltage waves are the most used in the WDF literature [7] and can be obtained setting ρ as

$$\rho = \begin{cases} 0 & \text{current waves} \\ 0.5 & \text{power waves} \\ 1 & \text{voltage waves} \end{cases} . \qquad (3)$$

A. Linear Elements

A large class of linear one-port elements, including resistors, resistive sources, and even capacitors and inductors [9], can be described by means of the following discrete-time Thévenin model

$$v[k] = R_{\mathrm{g}}[k]i[k] + V_{\mathrm{g}}[k], \qquad (4)$$

where k is the sampling index, $v[k]$ is the port voltage, $i[k]$ is the port current, $V_{\mathrm{g}}[k]$ is a voltage parameter, and $R_{\mathrm{g}}[k]$ is a resistive parameter. A general WD realization of such an element can be obtained substituting (2) into (4)

$$b[k] = \frac{R_{\mathrm{g}}[k] - Z[k]}{R_{\mathrm{g}}[k] + Z[k]} a[k] + \frac{2Z^{\rho}[k]}{R_{\mathrm{g}}[k] + Z[k]} V_{\mathrm{g}}[k]. \qquad (5)$$

If we set $Z[k] = R_{\mathrm{g}}[k]$, (5) reduces to

$$b[k] = R_{\mathrm{g}}^{\rho-1}[k]V_{\mathrm{g}}[k], \qquad (6)$$

thus removing the instantaneous dependence of $b[k]$ on $a[k]$: the element, in this case, is said to be *adapted* [7]. It is important to notice that the *adaptation condition* $Z[k] = R_{\mathrm{g}}[k]$ does not depend on ρ.

B. Nonlinear Elements

The constitutive equations of nonlinear circuit elements are often implicit, and thus, unlike linear one-ports, they cannot be adapted. Nevertheless, as demonstrated in [9], [13], the instantaneous dependence of $b[k]$ on $a[k]$ can be minimized by dynamically changing the port resistance in order to meet the slope of the tangent at the current operating point on the $i - v$ characteristic.

Diodes are the most common one-port nonlinear elements in audio circuits. Over the past few years, different techniques have been employed to model such elements in the WD domain, e.g., based on Newton-Raphson solvers [13], the Lambert $\mathcal{W}$ function [29], [30], or the Wright ω function [31].

Let us consider the *extended Shockley diode model* used in [9], [16], whose implicit equation is

$$f(v, i) = I_{\mathrm{s}}\left(\exp\left(\frac{v - R_{\mathrm{s}}i}{\eta V_{\mathrm{t}}}\right) - 1\right) + \frac{v - R_{\mathrm{s}}i}{R_{\mathrm{p}}} - i = 0, \quad (7)$$

where the sampling index k is omitted for the sake of clarity, I_{s} is the saturation current, η is the ideality factor, V_{t} is the thermal voltage, whereas R_{s} and R_{p} are the series and parallel resistances of the p-n junction. Making use of the parametric definition of waves (1), a possible WD realization of such a model is characterized by the following explicit scattering relation [31]

$$b = h(a) = \alpha - \beta \, \omega \left(\ln \gamma + \delta + \frac{\alpha}{\beta}\right), \qquad (8)$$

where $\omega(\cdot)$ is the Wright ω function, implemented as discussed in [32], and

$$
\begin{aligned}
\alpha &= \frac{2R_{\mathrm{p}}I_{\mathrm{s}} + a\left(Z^{-\rho}\left(R_{\mathrm{s}} + R_{\mathrm{p}}\right) - Z^{1-\rho}\right)}{Z^{1-\rho} + Z^{-\rho}\left(R_{\mathrm{s}} + R_{\mathrm{p}}\right)}, \\
\beta &= \frac{2\eta V_{\mathrm{t}}}{Z^{1-\rho} + R_{\mathrm{s}}Z^{-\rho}}, \\
\gamma &= \frac{R_{\mathrm{p}}I_{\mathrm{s}}(Z^{1-\rho} + R_{\mathrm{s}}Z^{-\rho})}{\eta V_{\mathrm{t}}\left(Z^{1-\rho} + Z^{-\rho}\left(R_{\mathrm{s}} + R_{\mathrm{p}}\right)\right)}, \\
\delta &= \frac{a(Z^{1-\rho} - R_{\mathrm{s}}Z^{-\rho})}{2\eta V_{\mathrm{t}}}.
\end{aligned}
\qquad (9)
$$

Let us now consider two identical diodes in antiparallel configuration, whose one-port extended Shockley model is shown in Fig. 1. The implicit equation that relates i to v is

$$g(v, i) = I_{\mathrm{s}}\left(\exp\left(\frac{v - R_{\mathrm{s}}i}{\eta V_t}\right) - \exp\left(\frac{-(v - R_{\mathrm{s}}i)}{\eta V_t}\right)\right) + \frac{v - R_{\mathrm{s}}i}{R_{\mathrm{p}}} - i = 0. \qquad (10)$$

As an approximation, considering only one diode to conduct at a time (i.e., the reverse current of the diode is negligible w.r.t. its forward current) and v and i sufficiently large in absolute value, we have

$$\exp\left(\frac{|v - R_{\mathrm{s}}i|}{\eta V_t}\right) \gg \exp\left(\frac{-|v - R_{\mathrm{s}}i|}{\eta V_t}\right). \qquad (11)$$

It follows that, by exploiting (11), the pair of antiparallel diodes can be implemented as a single one-port WD element with scattering relation

$$b = \mathrm{sgn}(a)h(|a|), \qquad (12)$$

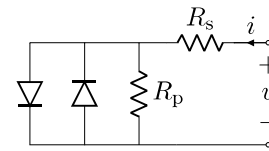where $\mathrm{sgn}(\cdot)$ is the sign function [29].

Fig. 1. Extended Shockley model of the antiparallel diodes considered in this work.

III. MODELING CONNECTION NETWORKS WITH NULLORS

Introduced in [24], [25], the nullor is a theoretical two-port element used in circuit theory to model the ideal behavior of several multi-ports, including active and nonreciprocal elements, such as transistors, opamps, controlled sources, etc. [26] As shown in Fig. 2, the nullor is composed of two one-port theoretical elements, the *nullator* and the *norator* [24], that do not have any physical meaning [25]. The nullator has both port voltage and port current equal to zero, whereas the norator shows unconstrained port variables, i.e., they can assume arbitrary values. The constitutive equation of a nullor is therefore

$$\begin{bmatrix} v_1 \\ i_1 \end{bmatrix} = \begin{bmatrix} 0 & 0 \\ 0 & 0 \end{bmatrix} \begin{bmatrix} v_2 \\ i_2 \end{bmatrix}, \qquad (13)$$
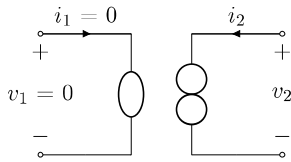
Fig. 2. Nullor circuit symbol. The nullator (port 1) is represented with an ellipse, while the norator (port 2) with two circles.

where v_1 and i_1 are the port voltage and the port current of the nullator port, while v_2 and i_2 are the port voltage and the port current of the norator port.

Our aim is to derive WD realizations of junctions including interconnections of nullors, which are often nonreciprocal [24]. It follows that the modeling approach dedicated to lossless reciprocal topological junctions, based on a *tree-cotree decomposition* [33] of the reference connection network and on the derivation of the corresponding fundamental loop and cut-set matrices [18], [19], cannot be used in these cases. In the next Subsection we show that, by considering a pair of directed graphs (digraphs) instead of just one as in [18], [19], we can still resort to a loop or cut-set analysis even if we deal with nonreciprocal connection networks containing nullors [34]. In fact, by solving the network for voltages, nullators behave like short circuits, whilst norators like open circuits. On the other hand, by solving the network for currents, the opposite holds true [26]. Moreover, we show that by combining the results of the two analyses, we can look at the initial problem as a set of linear independent homogeneous equations [34].

A. Fundamental Loop and Cut-set Analyses

Let us consider a nonreciprocal N-port connection network containing $L \geq 1$ nullors. Let us also assume that the nullors are the only elements absorbed in the connection network. Following the method proposed in [34], such a connection network can be described using two reciprocal N-port connection networks derived from it: the first (called *V-network*) with nullators replaced by short circuits and norators by open circuits, and the second (called *I-network*) with nullators replaced by open circuits and norators by short circuits. Naming $\mathbf{v} = [v_1, \ldots, v_N]^\mathrm{T}$ the vector of port voltages and $\mathbf{j} = [j_1, \ldots, j_N]^\mathrm{T}$ the vector of port currents, the Kirchhoff's laws can be thus represented in matrix form as

$$\begin{cases} \mathbf{j} = \mathbf{B}_\mathrm{I}^\mathrm{T} \mathbf{j}_\mathrm{l} \\ \mathbf{v} = \mathbf{Q}_\mathrm{V}^\mathrm{T} \mathbf{v}_\mathrm{t} \end{cases}, \qquad (14)$$

where $\mathbf{B}_\mathrm{I}$ is the fundamental loop matrix of the I-network of size $l \times N$, and $\mathbf{Q}_\mathrm{V}$ is the fundamental cut-set matrix of the V-network of size $t \times N$; moreover, $l + t = N$. In (14), $\mathbf{v}_\mathrm{t}$ is the vector of independent port voltages and $\mathbf{j}_\mathrm{l}$ the vector of independent port currents. Matrix $\mathbf{B}_\mathrm{I}$ and $\mathbf{Q}_\mathrm{V}$ can be formed by employing the tree-cotree digraph decomposition [18], [19], [33] of the two networks. The N branches of each oriented graph represent the ports of the connection network, and the

orientation of the arrows follows the same convention of the port currents. The branches are partitioned into two sets: t twigs (edges of a tree) and l links (edges of the relative cotree). Moreover, in order to make this double decomposition compliant with the reference circuit, the two digraphs must share the same tree.

By combining the outcomes of the two analyses, it is possible to write the Kirchhoff's laws as sets of independent homogeneous equations as [35]

$$\begin{aligned} \mathbf{Q}_\mathrm{V} \mathbf{j} = \mathbf{0}, && \mathbf{B}_\mathrm{V} \mathbf{v} = \mathbf{0}, \\ \mathbf{Q}_\mathrm{l} \mathbf{j} = \mathbf{0}, && \mathbf{B}_\mathrm{l} \mathbf{v} = \mathbf{0}, \end{aligned} \qquad (15)$$

where $\mathbf{B}_\mathrm{V}$ is the $l \times N$ fundamental loop matrix of the V-network and $\mathbf{Q}_\mathrm{I}$ is the $t \times N$ fundamental cut-set matrix of the I-network. In addition, given that the V-network and the I-network are reciprocal, the following orthogonality properties

$$\begin{aligned} \mathbf{B}_\mathrm{V} \mathbf{Q}_\mathrm{V}^\mathrm{T} = \mathbf{0}, && \mathbf{Q}_\mathrm{V} \mathbf{B}_\mathrm{V}^\mathrm{T} = \mathbf{0}, \\ \mathbf{B}_\mathrm{I} \mathbf{Q}_\mathrm{I}^\mathrm{T} = \mathbf{0}, && \mathbf{Q}_\mathrm{I} \mathbf{B}_\mathrm{I}^\mathrm{T} = \mathbf{0}, \end{aligned} \qquad (16)$$

hold true [35].

Starting from (14), we can write

$$\mathbf{Q}_\mathrm{V} = \begin{bmatrix} \hat{\mathbf{Q}}_\mathrm{V} & \mathbf{I} \end{bmatrix}, \qquad \mathbf{B}_\mathrm{I} = \begin{bmatrix} \mathbf{I} & \hat{\mathbf{B}}_\mathrm{I} \end{bmatrix}, \qquad (17)$$

where $\hat{\mathbf{Q}}_\mathrm{V}$ and $\hat{\mathbf{B}}_\mathrm{I}$ are matrices of size $t \times l$ and $l \times t$, respectively, and $\mathbf{I}$ is a properly sized identity matrix. Similarly, we can also write

$$\mathbf{Q}_\mathrm{I} = \begin{bmatrix} \hat{\mathbf{Q}}_\mathrm{I} & \mathbf{I} \end{bmatrix}, \qquad \mathbf{B}_\mathrm{V} = \begin{bmatrix} \mathbf{I} & \hat{\mathbf{B}}_\mathrm{V} \end{bmatrix}, \qquad (18)$$

where $\hat{\mathbf{Q}}_\mathrm{I}$ and $\hat{\mathbf{B}}_\mathrm{V}$ have again size $t \times l$ and $l \times t$, respectively. Substituting (17) and (18) in (16) yields

$$\begin{bmatrix} \hat{\mathbf{Q}}_\mathrm{V} & \mathbf{I} \end{bmatrix} \begin{bmatrix} \mathbf{I} \\ \hat{\mathbf{B}}_\mathrm{V}^\mathrm{T} \end{bmatrix} = \mathbf{0}, \qquad \begin{bmatrix} \hat{\mathbf{Q}}_\mathrm{I} & \mathbf{I} \end{bmatrix} \begin{bmatrix} \mathbf{I} \\ \hat{\mathbf{B}}_\mathrm{I}^\mathrm{T} \end{bmatrix} = \mathbf{0}, \qquad (19)$$

from which we derive the following identities

$$\hat{\mathbf{Q}}_\mathrm{V} = -\hat{\mathbf{B}}_\mathrm{V}^\mathrm{T}, \qquad \hat{\mathbf{Q}}_\mathrm{I} = -\hat{\mathbf{B}}_\mathrm{I}^\mathrm{T}. \qquad (20)$$

It follows that $\mathbf{Q}_\mathrm{V}$, $\mathbf{B}_\mathrm{V}$, $\mathbf{Q}_\mathrm{I}$, and $\mathbf{B}_\mathrm{I}$ can be expressed as functions of only two matrices, along the lines of what shown in [18] for reciprocal lossless connection networks. By setting $\hat{\mathbf{Q}}_\mathrm{V} = \mathbf{F}_\mathrm{V}$, $\hat{\mathbf{B}}_\mathrm{V} = -\mathbf{F}_\mathrm{V}^\mathrm{T}$, $\hat{\mathbf{Q}}_\mathrm{I} = \mathbf{F}_\mathrm{I}$, and $\hat{\mathbf{B}}_\mathrm{I} = -\mathbf{F}_\mathrm{I}^\mathrm{T}$, in fact, we have

$$\begin{aligned} \mathbf{Q}_\mathrm{V} = \begin{bmatrix} \mathbf{F}_\mathrm{V} & \mathbf{I} \end{bmatrix}, && \mathbf{B}_\mathrm{V} = \begin{bmatrix} \mathbf{I} & -\mathbf{F}_\mathrm{V}^\mathrm{T} \end{bmatrix}, \\ \mathbf{Q}_\mathrm{I} = \begin{bmatrix} \mathbf{F}_\mathrm{I} & \mathbf{I} \end{bmatrix}, && \mathbf{B}_\mathrm{I} = \begin{bmatrix} \mathbf{I} & -\mathbf{F}_\mathrm{I}^\mathrm{T} \end{bmatrix}. \end{aligned} \qquad (21)$$

This result is compliant with the intuition that the V-network and the I-network share a common set of independent variables [34].

As an explicative example, let us consider the circuit of the precision half-wave rectifier shown in Fig. 3(a), also known as *super diode*, and used in analog sound synthesizers to create low-frequency oscillations (LFOs) or controlled voltage (CV) waveforms. If we assume the opamp in Fig. 3(a) to be ideal, we can substitute it with its nullor-based equivalent [26]. Fig. 3(b) shows the 4-port topological connection network related to the circuit in Fig. 3(a) embedding the nullor-based opamp model. By replacing the nullator with a short circuit and the norator with an open circuit, we derive the V-network represented in Fig. 3(c). The I-network, instead, is shown in Fig. 3(d). The
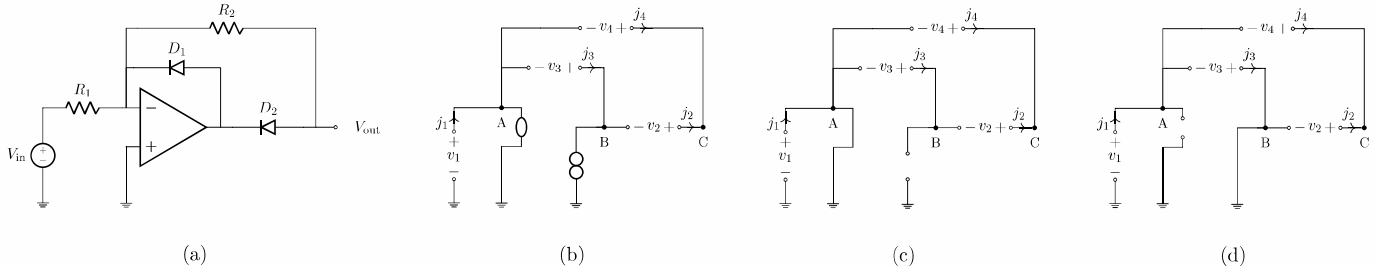
Fig. 3. (a) Precision half-wave rectifier (super diode). (b) Topological connection network of the circuit in (a) embedding the nullor-based model of the opamp; (c) V-network obtained from the connection network in (b) by replacing the nullator with a short circuit and the norator with an open circuit; (d) I-network obtained from the connection network in (b) by replacing the nullator with an open circuit and the norator with a short circuit.
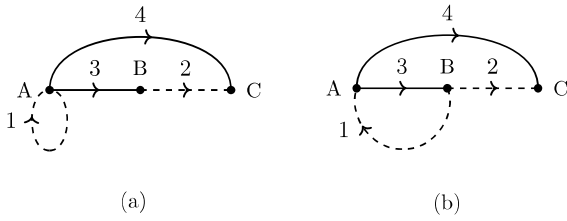

Fig. 4. (a) Tree-cotree decomposition of the V-network shown in Fig. 3(c); (b) Tree-cotree decomposition of the I-network shown in Fig. 3(d). The two oriented graphs share a common tree, represented with continuous lines, whereas the relative cotree is represented with dashed lines.

digraphs corresponding to the V-network and the I-network are shown in Fig. 4 where one possible common tree (continuous lines) and the associated cotree (dashed lines) are highlighted. Collected the independent port variables in the vectors $\mathbf{v}_t = [v_3, v_4]^{\mathrm{T}}$ and $\mathbf{j}_l = [j_1, j_2]^{\mathrm{T}}$, according to the performed tree-cotree digraph decomposition, the matrices $\mathbf{Q}_{\mathrm{V}}$, $\mathbf{B}_{\mathrm{V}}$, $\mathbf{Q}_{\mathrm{I}}$, and $\mathbf{B}_{\mathrm{I}}$ are formed using eq. (21), where

$$\mathbf{F}_{\mathrm{V}} = \begin{bmatrix} 0 & -1 \\ 0 & 1 \end{bmatrix}, \qquad \mathbf{F}_{\mathrm{I}} = \begin{bmatrix} -1 & -1 \\ 0 & 1 \end{bmatrix}, \qquad (22)$$

yielding

$$\mathbf{Q}_{\mathrm{V}} = \begin{bmatrix} 0 & -1 & 1 & 0 \\ 0 & 1 & 0 & 1 \end{bmatrix}, \quad \mathbf{B}_{\mathrm{V}} = \begin{bmatrix} 1 & 0 & 0 & 0 \\ 0 & 1 & 1 & -1 \end{bmatrix},$$

$$\mathbf{Q}_{\mathrm{I}} = \begin{bmatrix} -1 & -1 & 1 & 0 \\ 0 & 1 & 0 & 1 \end{bmatrix}, \quad \mathbf{B}_{\mathrm{I}} = \begin{bmatrix} 1 & 0 & 1 & 0 \\ 0 & 1 & 1 & -1 \end{bmatrix}. \quad (23)$$

B. Properties of the Scattering Matrix

A WD realization of an N-port topological junction embedding nullors is characterized by the scattering relation

$$\mathbf{b}_{\mathrm{J}} = \mathbf{S}\mathbf{a}_{\mathrm{J}}, \qquad (24)$$

where $\mathbf{S}$ is the so-called *scattering matrix*, while $\mathbf{a}_{\mathrm{J}}$ and $\mathbf{b}_{\mathrm{J}}$ are column vectors of length N collecting the waves incident to the junction and the waves reflected by the junction, respectively. Vectors $\mathbf{a}_{\mathrm{J}}$ and $\mathbf{b}_{\mathrm{J}}$ can be expressed as

$$\mathbf{a}_{\mathrm{J}} = \mathbf{Z}^{\rho-1}\mathbf{v} + \mathbf{Z}^{\rho}\mathbf{j}, \qquad \mathbf{b}_{\mathrm{J}} = \mathbf{Z}^{\rho-1}\mathbf{v} - \mathbf{Z}^{\rho}\mathbf{j}, \qquad (25)$$

where $\mathbf{Z} = \mathrm{diag}[Z_1, \ldots, Z_N]$ is a diagonal matrix having port resistances as non-zero entries.

As mentioned above, $\mathbf{v}$ and $\mathbf{j}$ are solutions of the sets of linear independent homogeneous equations in (15) (Kirchhoff's laws). Hence, being ξ and ζ arbitrary real numbers, even $\xi\mathbf{v}$ and $\zeta\mathbf{j}$ are solutions of the same systems of equations [35]. By substituting $\xi\mathbf{v}$ and $\zeta\mathbf{j}$ in (25) and then (25) in (24), we obtain

$$\xi\mathbf{Z}^{\rho-1}\mathbf{v} - \zeta\mathbf{Z}^{\rho}\mathbf{j} = \mathbf{S}\left(\xi\mathbf{Z}^{\rho-1}\mathbf{v} + \zeta\mathbf{Z}^{\rho}\mathbf{j}\right). \qquad (26)$$

By choosing $\xi = 1$ and $\zeta = -1$, it is evident that the relation $\mathbf{a}_{\mathrm{J}} = \mathbf{S}\mathbf{b}_{\mathrm{J}}$ must be true as well [36]. It follows that the scattering matrix $\mathbf{S}$ is an involutory matrix and the *self-inverse* property

$$\mathbf{S}\mathbf{S} = \mathbf{I} \qquad (27)$$

must be met. On the other hand, $\mathbf{S}$ does not satisfy the properties of *losslessness* and *reciprocity* [18], known, instead, to hold true for reciprocal lossless topological junctions.

C. Derivation of the Scattering Matrix

By substituting (14) into (25), we obtain

$$\mathbf{a}_{\mathrm{J}} = \mathbf{Z}^{\rho-1}\mathbf{Q}_{\mathrm{V}}^{\mathrm{T}}\mathbf{v}_t + \mathbf{Z}^{\rho}\mathbf{B}_{\mathrm{I}}^{\mathrm{T}}\mathbf{j}_l, \qquad (28)$$

$$\mathbf{b}_{\mathrm{J}} = \mathbf{Z}^{\rho-1}\mathbf{Q}_{\mathrm{V}}^{\mathrm{T}}\mathbf{v}_t - \mathbf{Z}^{\rho}\mathbf{B}_{\mathrm{I}}^{\mathrm{T}}\mathbf{j}_l. \qquad (29)$$

If we left-multiply both sides of (28) for $\mathbf{Q}_{\mathrm{I}}\mathbf{Z}^{-\rho}$ and both sides of (29) for $\mathbf{B}_{\mathrm{V}}\mathbf{Z}^{1-\rho}$ we get

$$\mathbf{Q}_{\mathrm{I}}\mathbf{Z}^{-\rho}\mathbf{a}_{\mathrm{J}} = \mathbf{Q}_{\mathrm{I}}\mathbf{Z}^{-1}\mathbf{Q}_{\mathrm{V}}^{\mathrm{T}}\mathbf{v}_t, \qquad (30)$$

$$\mathbf{B}_{\mathrm{V}}\mathbf{Z}^{1-\rho}\mathbf{b}_{\mathrm{J}} = -\mathbf{B}_{\mathrm{V}}\mathbf{Z}\mathbf{B}_{\mathrm{I}}^{\mathrm{T}}\mathbf{j}_l, \qquad (31)$$

respectively. By solving (30) for $\mathbf{v}_t$ and (31) for $\mathbf{j}_l$ we can write

$$\mathbf{v}_t = \left(\mathbf{Q}_{\mathrm{I}}\mathbf{Z}^{-1}\mathbf{Q}_{\mathrm{V}}^{\mathrm{T}}\right)^{-1}\mathbf{Q}_{\mathrm{I}}\mathbf{Z}^{-\rho}\mathbf{a}_{\mathrm{J}}, \qquad (32)$$

$$\mathbf{j}_l = -\left(\mathbf{B}_{\mathrm{V}}\mathbf{Z}\mathbf{B}_{\mathrm{I}}^{\mathrm{T}}\right)^{-1}\mathbf{B}_{\mathrm{V}}\mathbf{Z}^{1-\rho}\mathbf{b}_{\mathrm{J}}, \qquad (33)$$

which, once substituted into (28) and (29), lead to

$$\mathbf{a}_{\mathrm{J}} = \mathbf{Z}^{\rho-1}\mathbf{\Psi}\mathbf{Z}^{-\rho}\mathbf{a}_{\mathrm{J}} - \mathbf{Z}^{\rho}\mathbf{\Lambda}\mathbf{Z}^{1-\rho}\mathbf{b}_{\mathrm{J}}, \qquad (34)$$

$$\mathbf{b}_{\mathrm{J}} = \mathbf{Z}^{\rho-1}\mathbf{\Psi}\mathbf{Z}^{-\rho}\mathbf{a}_{\mathrm{J}} + \mathbf{Z}^{\rho}\mathbf{\Lambda}\mathbf{Z}^{1-\rho}\mathbf{b}_{\mathrm{J}}, \qquad (35)$$

where

$$\begin{aligned} \mathbf{\Psi} &= \mathbf{Q}_{\mathrm{V}}^{\mathrm{T}}\left(\mathbf{Q}_{\mathrm{I}}\mathbf{Z}^{-1}\mathbf{Q}_{\mathrm{V}}^{\mathrm{T}}\right)^{-1}\mathbf{Q}_{\mathrm{I}}, \\ \mathbf{\Lambda} &= \mathbf{B}_{\mathrm{I}}^{\mathrm{T}}\left(\mathbf{B}_{\mathrm{V}}\mathbf{Z}\mathbf{B}_{\mathrm{I}}^{\mathrm{T}}\right)^{-1}\mathbf{B}_{\mathrm{V}}. \end{aligned} \qquad (36)$$

TABLE I
FORMATION OF THE SCATTERING MATRIX OF A GENERAL JUNCTION EMBEDDING NULLORS:
COMPUTATIONAL COST COMPARISON BETWEEN THE PROPOSED METHOD AND THE MNA-BASED METHOD PRESENTED IN [17].
PARAMETER ρ REPRESENTS THE WAVE TYPE, WHEREAS K THE NUMBER OF CIRCUIT NODES.

Circuit Name	Size of Matrix to be inverted		Cost of Scattering in Multiplies			
	$\forall \rho$		$\rho \neq 0 \wedge \rho \neq 1$		$\rho = 0 \vee \rho = 1$	
	Proposed Method	MNA-based Method	Proposed Method	MNA-based Method	Proposed Method	MNA-based Method
General N-port with L Nullors	$\min\{t \times t, l \times l\}$	$(K-1+L) \times (K-1+L)$	$\min\{2N+t^2, 2N+l^2\}$	$2N+(K-1)^2$	$\min\{N+t^2, N+l^2\}$	$N+(K-1)^2$
Precision Rectifier Fig. 3(a)	2×2	4×4	12	17	8	13
Sallen-Key Filter Fig. 5(a)	2×2	5×5	14	26	9	21
Biquad Filter Fig. 5(b)	4×4	10×10	34	67	25	58

Finally, the scattering matrix $\mathbf{S}$ can be computed by adding (34) to (35) and solving for $\mathbf{b}_J$ as

$$\mathbf{S} = 2\mathbf{Z}^{\rho-1}\boldsymbol{\Psi}\mathbf{Z}^{-\rho} - \mathbf{I}, \tag{37}$$

or by subtracting (34) from (35) and solving for $\mathbf{a}_J$ as

$$\mathbf{S} = \mathbf{I} - 2\mathbf{Z}^{\rho}\boldsymbol{\Lambda}\mathbf{Z}^{1-\rho}. \tag{38}$$

In fact, thanks to the involutority property (27), eqs. (37) and (38) are two equivalent expressions. It is worth noticing that, if $l > t$, (37) is computationally cheaper than (38), since it entails the inversion of $\boldsymbol{\Psi}$ ($t \times t$ matrix) rather than $\boldsymbol{\Lambda}$ ($l \times l$ matrix). On the other hand, if $t > l$ the opposite holds true. Then, it is worth pointing out that, if $\mathbf{Q}_V = \mathbf{Q}_I$ and $\mathbf{B}_V = \mathbf{B}_I$, (37) and (38) reduce to the formulas derived in [18] for reciprocal lossless topological junctions. As a final remark, since some pathological interconnections of nullors might lead to unsolvable networks [37], the matrices $\mathbf{Q}_I\mathbf{Z}^{-1}\mathbf{Q}_V^T$ and $\mathbf{B}_V\mathbf{Z}\mathbf{B}_I^T$ could be singular. In those cases, the scattering matrix cannot be computed following this approach.

D. Computational Cost Comparison with MNA-based Method

The state-of-the-art method for computing the scattering matrix of a topological junction embedding nullors, to which we will compare the method proposed in the previous subsection, is presented in [17] and it is based on the MNA approach. According to [17], the scattering matrix $\mathbf{S}$ can be computed as (see eq. (23) and eq. (27) in [17])

$$\mathbf{S} = 2\mathbf{Z}^{\rho-1}\tilde{\mathbf{A}}_p^T [\mathbf{I}\ \mathbf{0}] \tilde{\mathbf{X}}_0^{-1} [\mathbf{I}\ \mathbf{0}]^T \tilde{\mathbf{A}}_p \mathbf{Z}^{-\rho} - \mathbf{I}, \tag{39}$$

where $\mathbf{I}$ indicates an identity matrix of proper size, $\mathbf{0}$ is a zero matrix of proper size, $\tilde{\mathbf{X}}_0$ is a reduced version of the extended nodal matrix from which the kth column and the kth row have been removed, whereas $\tilde{\mathbf{A}}_p$ is a reduced version of the port incidence matrix from which the kth row has been removed, as explained in [17].

As shown in Table I, the computational cost comparison between the proposed method and the MNA-based method considers both the size of the matrix to be inverted in order to form $\mathbf{S}$ and the cost of scattering in multiplies, which is the number of multiplications involving the defining terms of
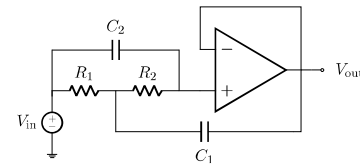
(a)
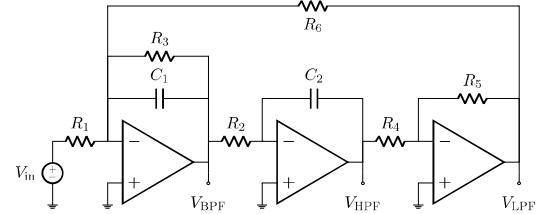
(b)

Fig. 5. (a) Unity-gain Sallen-Key low-pass filter; (b) Biquad filter composed of three opamps: V_{BPF} is the output of the band-pass filter, V_{HPF} is the output of the high-pass filter, and V_{LPF} is the output of the low-pass filter.

$\mathbf{S}$ and required to compute $\mathbf{b}_J$ given $\mathbf{a}_J$ in accordance to (24). Following what done in Table III of [17], the cost is evaluated assuming that all matrices in eqs. (37), (38), and (39) have been already computed. The matrix to be inverted using the proposed method is either $\mathbf{Q}_I\mathbf{Z}^{-1}\mathbf{Q}_V^T$ or $\mathbf{B}_V\mathbf{Z}\mathbf{B}_I^T$, depending on which one has a smaller size, while using the MNA-method it is $\tilde{\mathbf{X}}_0$. Being K the number of nodes of the circuit and L the number of nullors, the size of $\tilde{\mathbf{X}}_0$ is $(K-1+L) \times (K-1+L)$, hence, it quadratically increases with the number of nullors. The method proposed in this manuscript, instead, is more cost-effective since it entails the inversion of a $t \times t$ or $l \times l$ matrix that is always smaller than $\tilde{\mathbf{X}}_0$ in size. General formulas of the cost in multiplies for performing the scattering are also reported in Table I.

As examples, along with the already discussed precision rectifier circuit in Fig. 3(a), we consider other two circuits widely spread in audio systems: a Sallen-Key low-pass filter [38] and a Biquad filter (universal filter) [39], represented

in Fig. 5(a) and Fig. 5(b), respectively. As for the precision half-wave rectifier circuit, also in these cases, the opamps are substituted with their nullor-based models. The connection network of the Sallen-Key filter circuit is characterized by 5 ports that are, in order, connected to one-port elements: C_1, C_2, V_{in}, R_1, and R_2. The fundamental loop and cut-set matrices of the V- and I-networks obtained from the connection network can be computed by substituting in (21) the following matrices

$$\mathbf{F}_V = \begin{bmatrix} 0 & 0 \\ 0 & -1 \\ -1 & -1 \end{bmatrix}, \quad \mathbf{F}_I = \begin{bmatrix} 1 & 0 \\ 1 & -1 \\ 0 & -1 \end{bmatrix}. \quad (40)$$

The connection network of the Biquad filter circuit is characterized by 10 ports that are, in order, connected to one-port elements: V_{in}, R_3, R_2, R_6, R_4, R_1, C_1, C_2, and R_5. In this case, matrices $\mathbf{F}_V$ and $\mathbf{F}_I$ are

$$\mathbf{F}_V = \begin{bmatrix} 1 & 0 & 0 & 0 & 0 \\ 0 & 1 & 1 & 0 & 0 \\ 0 & 0 & 0 & 0 & -1 \\ 0 & 0 & 0 & -1 & 0 \end{bmatrix},$$

$$(41)$$

$$\mathbf{F}_I = \begin{bmatrix} 1 & 0 & 0 & 0 & 0 \\ 1 & 1 & 0 & 1 & 0 \\ 0 & 0 & -1 & 0 & 0 \\ 0 & 0 & 0 & 0 & -1 \end{bmatrix}.$$

Table I shows the results of the comparison for the three considered examples. We can notice that the proposed method is always computationally more convenient than the MNA-based method. This fact is particularly promising in the context of the SIM algorithm for solving circuits with multiple nonlinearities in the WD domain that requires to frequently update the scattering junction matrix, as we will extensively discuss in the next sections.

IV. SCATTERING ITERATIVE METHOD

Introduced in [13] for the static analysis of large photo-voltaic arrays, and later employed in [9], [16] for the emulation of dynamic audio circuits, the Scattering Iterative Method (SIM) is a WD iterative method for the simulation of circuits containing multiple nonlinearities.

Similarly to what done in [9], [16], we assume that the circuit is modeled in the WD domain using a single multi-port scattering junction to which all the elements are connected. Let us name $\mathbf{a} = [a_1, \ldots, a_N]^T$ the vector of waves incident to the elements (reflected by the junction) and $\mathbf{b} = [b_1, \ldots, b_N]^T$ the vector of waves reflected by the elements (incident to the junction). It follows that the vector of port voltages $\mathbf{v}$ is the same of Section III, whereas the vector of port currents of the elements $\mathbf{i}$ is defined as $\mathbf{i} = -\mathbf{j}$, yielding $\mathbf{a} = \mathbf{b}_J$ and $\mathbf{b} = \mathbf{a}_J$. In order to find a solution to the nonlinear circuit in the WD domain at a generic sampling step (indicated with the sampling index k) of the discrete-time simulation, the SIM algorithm performs the following four stages in an iterative fashion:

1) *Initialization and Update*: the free parameters $Z_1[k], \ldots, Z_N[k]$ are set as close as possible to

the tangent slope at the current working point on the $i - v$ characteristic. For linear elements, this is straightforward and can be achieved employing the adaptation conditions known in traditional WDFs [7]. For nonlinear one-ports, instead, optimal slopes can only be estimated as a function of $i_n[k - 1]$ and $v_n[k - 1]$, i.e., the values of the nth port current and port voltage at the operating point of the previous sample. Moreover, if the free parameters are varied, the scattering matrix $\mathbf{S}$ must be updated (using the formulas discussed in the previous section).

2) *Local Scattering Stage*: the waves $b_n^{(\gamma)}[k]$, in case they are reflected by adapted linear elements, are computed as in (6), whereas in case they are reflected by one-port nonlinear elements as

$$b_n^{(\gamma)}[k] = f_n(a_n^{(\gamma-1)}[k]) \quad (42)$$

where γ is the fixed-point index, and the generic non-linear function $f_n(\cdot)$ indicates the WD mapping (see e.g., (8) and (12)) employed to model the element connected to port n.

3) *Global Scattering Stage*: the vector $\mathbf{a}^{(\gamma)}[k]$ of the waves incident to the elements can be computed as follows

$$\mathbf{a}^{(\gamma)}[k] = \mathbf{S}[k]\mathbf{b}^{(\gamma)}[k]. \quad (43)$$

4) *Convergence Check*: Local Scattering Stage and Global Scattering Stage are reiterated until the inequality

$$\|\mathbf{v}^{(\gamma)}[k] - \mathbf{v}^{(\gamma-1)}[k]\|_2 < \varepsilon_{SIM} \quad (44)$$

holds true, where $\mathbf{v}^{(\gamma)}[k] = (\mathbf{a}^{(\gamma)}[k] + \mathbf{b}^{(\gamma)}[k])/2$ and ε_{SIM} is a small threshold (e.g., $\varepsilon_{SIM} = 10^{-5}$).

The scattering matrix $\mathbf{S}$ is usually recomputed at each sampling step k. Hence, when dealing with networks containing nullors, a careful choice of the technique used to compute $\mathbf{S}$ (among those discussed in Section III) can really make the difference in terms of computational complexity, as we will show in some examples of application in Section V.

A. Convergence Analysis

In the literature [9], [13], it has been shown that SIM always converges to the correct circuit solution, under the following assumptions:

- the free parameters are positive (i.e., $Z_n[k] > 0 \ \forall \ n, k$);
- each circuit elements is characterized by a monotonically increasing $i - v$ characteristic;
- the junction is lossless and reciprocal.

In this manuscript, we consider the more general case in which the connection network embeds nullors; hence, the resulting WD junction might be nonreciprocal and/or nonlossless. This means that we cannot rely on the reciprocity and losslessness properties of $\mathbf{S}$ [18], which have been extensively used to derive a proof of SIM convergence in [13], [40]. In the light of this, in the following we provide some considerations on the convergence properties of SIM, when it is applied to WD structures characterized by nonreciprocal topological junctions containing nullors.

SIM is a fixed-point method and, by combining (42) and (43), its update formula at each fixed-point iteration can be expressed in a compact fashion as

$$\mathbf{a}^{(\gamma)} = \mathbf{S}\mathbf{f}\left(\mathbf{a}^{(\gamma-1)}\right), \qquad (45)$$

where, for the sake of clarity, the sampling index k has been removed and $\mathbf{f}(\mathbf{a}) = [f_1(a_1), \ldots, f_N(a_N)]^{\mathrm{T}}$ is the vector of scattering functions related to the one-port elements. It is worth noticing that here f_n indicates either a linear or a nonlinear scattering function (e.g., (6), (8) or (12)). Let us indicate the $i - v$ characteristic of each element as $v_n(i_n)$. Moreover, we consider it to be continuous and differentiable $\forall\, i_n \in \mathbb{R}$. As already shown in [40], [41], it is convenient to rewrite (1) as

$$a_n = Z_n^{\rho-1} v_n(i_n) + Z_n^\rho i_n = \phi_n(i_n), \qquad (46)$$
$$b_n = Z_n^{\rho-1} v_n(i_n) - Z_n^\rho i_n = \psi_n(i_n). \qquad (47)$$

Assuming that $\phi_n(i_n)$ is invertible, we can write the generic scattering relation of the nth circuit element as

$$b_n = f_n(a_n) = \psi_n(\phi_n^{-1}(a_n)). \qquad (48)$$

The derivative of (48) with respect to a_n can be then assessed via

$$f_n'(a_n) = \frac{\psi_n'(\phi_n^{-1}(a_n))}{\phi_n'(\phi_n^{-1}(a_n))} = \frac{v_n'(i_n) - Z_n}{v_n'(i_n) + Z_n}, \qquad (49)$$

where $v_n'(i_n)$ is the derivative of $v_n(i_n)$ with respect to i_n. It follows that the Jacobian matrix of $\mathbf{f}(\mathbf{a})$ can be expressed as

$$\mathbf{J_f}(\mathbf{a}) = \begin{bmatrix} f_1'(a_1) & & \mathbf{0} \\ & \ddots & \\ \mathbf{0} & & f_N'(a_N) \end{bmatrix} = \begin{bmatrix} \frac{v_1'(i_1) - Z_1}{v_1'(i_1) + Z_1} & & \mathbf{0} \\ & \ddots & \\ \mathbf{0} & & \frac{v_N'(i_N) - Z_N}{v_N'(i_N) + Z_N} \end{bmatrix}. \qquad (50)$$

According to (45), as extensively discussed in [40], a sufficient condition for SIM to converge is

$$\mathrm{srad}\left(\mathbf{S}\mathbf{J_f}(\mathbf{a})\right) < 1, \quad \forall\, \mathbf{a} \in \mathbb{R}^N, \qquad (51)$$

where the operator $\mathrm{srad}(\cdot)$ returns the spectral radius (i.e., the maximum eigenvalue in modulus) of the matrix in the argument. Given that each $v_n(i_n)$ is monotonically increasing, i.e., $v_n'(i_n) > 0$, and that each free parameter Z_n is positive (in fact, typically we set $Z_n[k] = v_n'(i_n[k-1])$), the entries of $\mathbf{J_f}(\mathbf{a})$ are all less than one in absolute value, i.e.,

$$|f_n'(a_n)| < 1, \quad \forall\, n = 1, \ldots, N. \qquad (52)$$

As a consequence, we have that

$$\mathrm{srad}\left(\mathbf{J_f}(\mathbf{a})\right) < 1, \quad \forall\, \mathbf{a} \in \mathbb{R}^N. \qquad (53)$$

Let us assume, without loss of generality, that the nonlinear elements of the circuit are connected to the first P ports of the N-port scattering junction, where $1 \le P \le N$. The scattering matrix $\mathbf{S}$ can be thus expressed in block matrix form as

$$\mathbf{S} = \begin{bmatrix} \mathbf{S_{11}} & \mathbf{S_{12}} \\ \mathbf{S_{21}} & \mathbf{S_{22}} \end{bmatrix}, \qquad (54)$$

where $\mathbf{S_{11}}$ is a $P \times P$ matrix, $\mathbf{S_{12}}$ is a $P \times (N-P)$ matrix, $\mathbf{S_{21}}$ is a $(N-P) \times P$ matrix, and $\mathbf{S_{22}}$ is a $(N-P) \times$

$(N-P)$ matrix. Assuming that all linear elements are adapted, the corresponding free parameters are set as $Z_n = v_n'(i_n) = R_{gn}$ at each sampling step, where R_{gn} is known and does not depend on i_n [9]. It follows that, according to (49) and (50), the diagonal entries of $\mathbf{J_f}(\mathbf{a})$ with indexes $P+1, \ldots, N$ are zero, and we can write

$$\mathbf{J_f}(\mathbf{a}) = \begin{bmatrix} \mathbf{J_{f11}}(\mathbf{a}) & \mathbf{0} \\ \mathbf{0} & \mathbf{0} \end{bmatrix}, \qquad (55)$$

where $\mathbf{J_{f11}}(\mathbf{a})$ collects the first P diagonal entries of $\mathbf{J_f}(\mathbf{a})$. Since the block matrix

$$\mathbf{S}\mathbf{J_f}(\mathbf{a}) = \begin{bmatrix} \mathbf{S_{11}}\mathbf{J_{f11}}(\mathbf{a}) & \mathbf{0} \\ \mathbf{S_{21}}\mathbf{J_{f11}}(\mathbf{a}) & \mathbf{0} \end{bmatrix} \qquad (56)$$

has a block of zeros in the counter-diagonal, we have that

$$\mathrm{srad}\left(\mathbf{S}\mathbf{J_f}(\mathbf{a})\right) = \mathrm{srad}\left(\mathbf{S_{11}}\mathbf{J_{f11}}(\mathbf{a})\right). \qquad (57)$$

By considering the properties of the spectral radius and the Schwarz inequality, it is possible to find an upper bound to (57) as follows

$$\mathrm{srad}\left(\mathbf{S_{11}}\mathbf{J_{f11}}(\mathbf{a})\right) \le \|\mathbf{S_{11}}\mathbf{J_{f11}}(\mathbf{a})\|_2 \le \|\mathbf{S_{11}}\|_2\|\mathbf{J_{f11}}(\mathbf{a})\|_2. \qquad (58)$$

Since $\mathbf{J_{f11}}(\mathbf{a})$ is a diagonal matrix, we have that $\|\mathbf{J_{f11}}(\mathbf{a})\|_2 = \mathrm{srad}(\mathbf{J_{f11}}(\mathbf{a}))$; moreover, the inequality $\mathrm{srad}(\mathbf{J_{f11}}(\mathbf{a})) < 1$ holds true since $\mathrm{srad}(\mathbf{J_f}(\mathbf{a})) < 1$. SIM convergence thus depends on the 2-norm of $\mathbf{S_{11}}$, raising interest in the properties of such a submatrix. In particular, if the inequality

$$\|\mathbf{S_{11}}\|_2 \mathrm{srad}(\mathbf{J_{f11}}(\mathbf{a})) < 1 \qquad (59)$$

holds true, then SIM convergence is ensured.

Let us define $\tilde{\mathbf{Q}}_{\mathrm{V}}$, $\tilde{\mathbf{B}}_{\mathrm{V}}$, $\tilde{\mathbf{Q}}_{\mathrm{I}}$, and $\tilde{\mathbf{B}}_{\mathrm{I}}$ as the matrices collecting the first P columns of $\mathbf{Q}_{\mathrm{V}}$, $\mathbf{B}_{\mathrm{V}}$, $\mathbf{Q}_{\mathrm{I}}$, and $\mathbf{B}_{\mathrm{I}}$, respectively, and $\tilde{\mathbf{Z}}$ as the diagonal matrix collecting the first P diagonal entries of $\mathbf{Z}$, i.e., gathering all the free parameters of the nonlinear one-ports. It is possible then to directly compute $\mathbf{S_{11}}$ from the loop/cut-set analysis of the connection network embedding nullors employing one of the two following formulas, derived from (37) and (38), respectively,

$$\mathbf{S_{11}} = 2\tilde{\mathbf{Z}}^{\rho-1}\tilde{\mathbf{Q}}_{\mathrm{V}}^{\mathrm{T}}\left(\mathbf{Q}_{\mathrm{I}}\mathbf{Z}^{-1}\mathbf{Q}_{\mathrm{V}}^{\mathrm{T}}\right)^{-1}\tilde{\mathbf{Q}}_{\mathrm{I}}\tilde{\mathbf{Z}}^{-\rho} - \mathbf{I},$$
$$\mathbf{S_{11}} = \mathbf{I} - 2\tilde{\mathbf{Z}}^\rho\tilde{\mathbf{B}}_{\mathrm{I}}^{\mathrm{T}}\left(\mathbf{B}_{\mathrm{V}}\mathbf{Z}\mathbf{B}_{\mathrm{I}}^{\mathrm{T}}\right)^{-1}\tilde{\mathbf{B}}_{\mathrm{V}}\tilde{\mathbf{Z}}^{1-\rho}. \qquad (60)$$

In general, matrix $\mathbf{S_{11}}$ is not involutory as $\mathbf{S}$, i.e., $\mathbf{S_{11}}\mathbf{S_{11}} \ne \mathbf{I}$. However, we can still exploit (60) to derive some interesting properties of $\mathbf{S_{11}}$. For construction, the digraphs of the V- and I-network are very similar, since the only differences lie where the nullors are placed. As a consequence, both the pair of matrices $\mathbf{Q}_{\mathrm{V}}$ and $\mathbf{Q}_{\mathrm{I}}$ and the pair of matrices $\mathbf{B}_{\mathrm{V}}$ and $\mathbf{B}_{\mathrm{I}}$ have often some identical columns. By exploiting the property of matrix congruence, it can be verified that if the two matrices $\tilde{\mathbf{Z}}^{\rho-1}\tilde{\mathbf{Q}}_{\mathrm{V}}^{\mathrm{T}}$ and $\tilde{\mathbf{Q}}_{\mathrm{I}}\tilde{\mathbf{Z}}^{-\rho}$ or the two matrices $\tilde{\mathbf{Z}}^\rho\tilde{\mathbf{B}}_{\mathrm{I}}^{\mathrm{T}}$ and $\tilde{\mathbf{B}}_{\mathrm{V}}\tilde{\mathbf{Z}}^{1-\rho}$ are symmetric, then also $\mathbf{S_{11}}$ is symmetric. In the cases in which $\tilde{\mathbf{Q}}_{\mathrm{V}} = \tilde{\mathbf{Q}}_{\mathrm{I}}$ or $\tilde{\mathbf{B}}_{\mathrm{V}} = \tilde{\mathbf{B}}_{\mathrm{I}}$, matrix $\mathbf{S_{11}}$ is always symmetric when $\rho = 0.5$. If, instead, one of the two conditions is not verified, $\mathbf{S_{11}}$ is, in general, not symmetric for any value of ρ. The symmetry of $\mathbf{S_{11}}$ would be a useful property since it would allow us to recast the convergence criterion. In fact, if
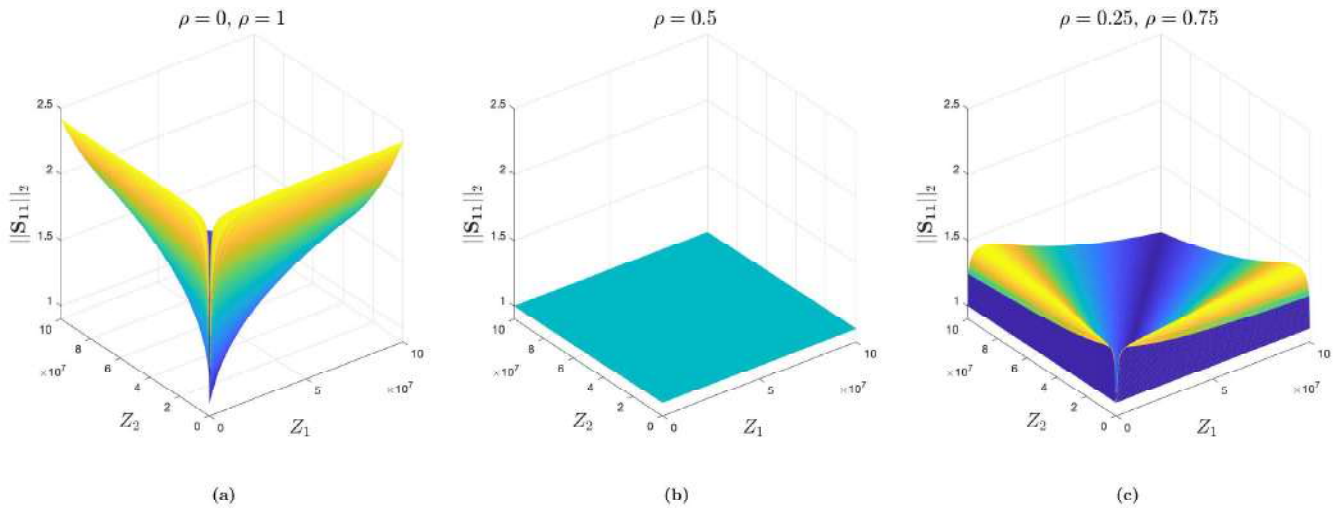
Fig. 6. Precision half-wave rectifier: Euclidian norm (or 2-norm) of matrix $\mathbf{S_{11}}$ as a function of port resistances Z_1 and Z_2 and of wave parameter ρ. (a) norm $\|\mathbf{S_{11}}\|_2$ considering $\rho = 0$ or $\rho = 1$; (b) norm $\|\mathbf{S_{11}}\|_2$ considering $\rho = 0.5$; (c) norm $\|\mathbf{S_{11}}\|_2$ considering $\rho = 0.25$ or $\rho = 0.75$. For $\rho = 0.5$, matrix $\mathbf{S_{11}}$ is symmetric, and, as a consequence, the norm assumes a constant value, being thus independent of Z_1 and Z_2.

$\mathbf{S_{11}}$ is symmetric, then $\|\mathbf{S_{11}}\|_2 = \mathrm{srad}(\mathbf{S_{11}})$ and (59) can be written as

$$\mathrm{srad}(\mathbf{S_{11}})\mathrm{srad}(\mathbf{J_{f11}}(\mathbf{a})) < 1. \qquad (61)$$

As a final remark, it is worth noticing that the smaller the left-hand side of (59) the higher the speed of SIM convergence; hence, the smaller $\|\mathbf{S_{11}}\|_2$ and $\mathrm{srad}(\mathbf{J_{f11}}(\mathbf{a}))$ the better. As a significant example, we notice that if the reference circuit is linear and all the elements are adapted we have that $\mathrm{srad}(\mathbf{J_{f11}}(\mathbf{a})) = 0$ and SIM converges in one iteration.

V. EXAMPLES OF APPLICATION

In this Section, we apply the proposed method for the WD simulation of two audio circuits. The accuracy check is performed by comparing the results of the WD implementations to those of LTspice (a widely used freeware Spice-like simulator). We then draw a comparison between the performance of SIM employing the MNA-based technique [17] for the computation of scattering matrices absorbing nullors and the performance of SIM employing, instead, the proposed double-digraph method, highlighting the perks of such a novel approach.
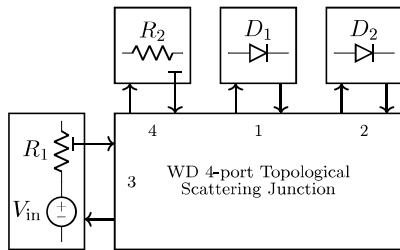

Fig. 7. A possible WD realization of the circuit shown in Fig. 3. The T-shaped stubs indicate port adaptation.

A. Precision Half-Wave Rectifier

As a first example, let us consider the precision half-wave rectifier shown in Fig. 3(a) and already analyzed in Subsection III-C. This circuit is part of many analog audio systems, including the SIGN section of the Kinks Eurorack module, produced by Mutable Instruments [43]. Resistances are set as $R_1 = 200$ kΩ and $R_2 = 100$ kΩ, whereas the 1N4148 diodes are described using the extended Shockley model of Subsection II-B, whose parameters are $R_\mathrm{s} = 1$ mΩ, $R_\mathrm{p} = 100$ MΩ, $I_\mathrm{s} = 4.352$ nA, $V_\mathrm{t} = 25.85$ mV, and $\eta = 1.905$. As input signal, we consider a sinusoidal voltage $V_\mathrm{in}[k] = A \sin(2\pi k f_0/f_\mathrm{s})$, where k is the sampling index, $A = 5$ V is the amplitude, $f_0 = 500$ Hz is the signal frequency, and $f_\mathrm{s} = 44.1$ kHz is the sampling frequency. The WD implementation of the considered circuit is shown in Fig. 7, where all the one-ports are connected to a single WD topological junction. The free parameters of linear elements are set to meet the relative adaptation condition, while those of nonlinear elements are set to match the tangent slope of their $i - v$ characteristic at the operating point of the previous sample. As shown in Subsection III-C, if we assume the opamp to be ideal, we can substitute it with its nullor equivalent, and apply the method explained in Section III to derive the scattering junction matrix $\mathbf{S}$. We perform the cut-set analysis and employ (37) to compute $\mathbf{S}$. Let us reorder the ports of the junction in a different way w.r.t. what done in Subsection III-C, such that port number 1 and port number 2 are connected to the two diodes. Matrices $\mathbf{Q_V}$ and $\mathbf{Q_I}$ are redefined by changing the order of their columns accordingly as

$$\mathbf{Q_V} = \begin{bmatrix} 1 & -1 & 0 & 0 \\ 0 & 1 & 0 & 1 \end{bmatrix}, \quad \mathbf{Q_I} = \begin{bmatrix} 1 & -1 & -1 & 0 \\ 0 & 1 & 0 & 1 \end{bmatrix}. \qquad (62)$$

Therefore, following the conventions introduced in Subsection IV-A, matrices $\tilde{\mathbf{Q}}_\mathrm{V}$ and $\tilde{\mathbf{Q}}_\mathrm{I}$ are

$$\tilde{\mathbf{Q}}_\mathrm{V} = \begin{bmatrix} 1 & -1 \\ 0 & 1 \end{bmatrix}, \quad \tilde{\mathbf{Q}}_\mathrm{I} = \begin{bmatrix} 1 & -1 \\ 0 & 1 \end{bmatrix}, \qquad (63)$$
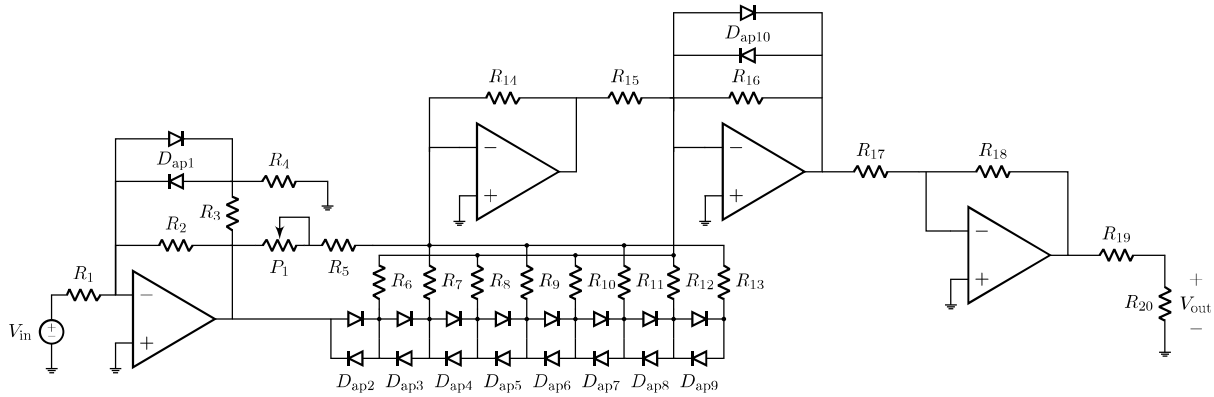
Fig. 8. Circuit schematic of a wave folder inspired to Wave Multiplier B by J. Haible [42].

and can be substituted into (60) in order to compute matrix $\mathbf{S_{11}}$. The eigenvalues of $\mathbf{S_{11}}$ can be expressed as functions of the reference port resistances as

$$\lambda_1(\mathbf{S_{11}}) = 1, \qquad \lambda_2(\mathbf{S_{11}}) = -\frac{Z_1 + Z_2 - Z_4}{Z_1 + Z_2 + Z_4}, \qquad (64)$$

where Z_1, Z_2, and Z_4 are the free parameters of diode D_1, diode D_2, and resistor R_2, respectively. Moreover, we notice that $\lambda_1(\mathbf{S_{11}})$ and $\lambda_2(\mathbf{S_{11}})$ are independent of ρ. As pointed out in Subsection IV-A, since $\tilde{\mathbf{Q}}_V = \tilde{\mathbf{Q}}_I$, matrix $\mathbf{S_{11}}$ is symmetric when $\rho = 0.5$. Hence, in this case, according to (64) we have that $\|\mathbf{S_{11}}\|_2 = \mathrm{srad}(\mathbf{S_{11}}) = 1$, therefore SIM convergence is assured. A further study on the 2-norm of $\mathbf{S_{11}}$ is shown in Fig. 6. In particular, $\|\mathbf{S_{11}}\|_2$ is plotted as a function of Z_1 and Z_2. Five values of ρ are taken into account: $\rho = 0$, $\rho = 0.25$, $\rho = 0.5$, $\rho = 0.75$, and $\rho = 1$. It turns out that, in this example, the values of $\|\mathbf{S_{11}}\|_2$ for $\rho = 0$ and $\rho = 1$ are the same and they are reported in Fig. 6(a); the result for $\rho = 0.5$ is shown in Fig. 6(b), whereas Fig. 6(c) reports the results for $\rho = 0.25$ and $\rho = 0.75$ that are also the same. We notice that for $\rho = 0.5$ we always have $\|\mathbf{S_{11}}\|_2 = 1$ independently of Z_1 and Z_2, confirming the aforementioned considerations.

The output signal of the circuit is the voltage across resistor R_2. Fig. 9 shows that the results obtained with the implemented WDF and the LTspice result are practically indistinguishable. Finally, with the purpose of comparing the performance of SIM coupled to the MNA-based approach for computing $\mathbf{S}$ [17] and SIM coupled to the proposed double-digraph approach, 100 identical runs of 5 s of simulation are performed (in the MATLAB 2020 environment on a standard Intel i5-core processor), and the average simulation time t_{sim} is then computed. Table II shows the results of such a comparison for three different values of wave parameter ρ: $\rho = 0$, $\rho = 0.5$, and $\rho = 1$. For all the three cases, with the proposed approach, a noticeable improvement in terms of SIM performance can be appreciated even dealing with such a small circuit.

B. Wave Folder

Let us now consider the circuit shown in Fig. 8 representing a wave folder inspired to Wave Multiplier B by J. Haible
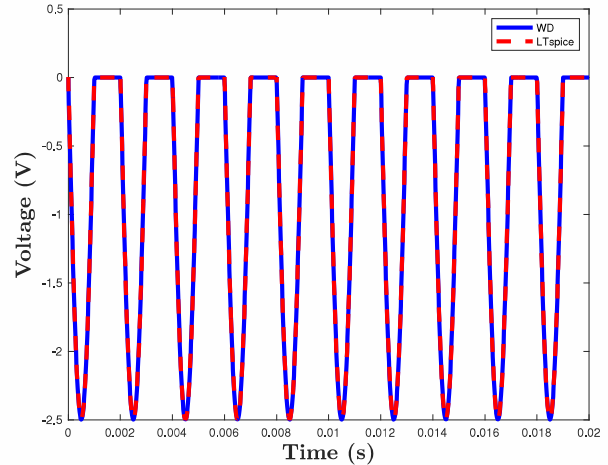

Fig. 9. Output voltage of the precision half-wave rectifier shown in Fig. 3. The blue curve represents the WD implementation, whereas the dashed red curve the LTspice implementation.

TABLE II
PRECISION HALF-WAVE RECTIFIER: COMPARISON BETWEEN THE
AVERAGE SIMULATION TIME OF SIM COUPLED TO THE PROPOSED
APPROACH AND TO THE MNA-BASED APPROACH FOR DIFFERENT
VALUES OF ρ.

	$\rho = 0$	$\rho = 0.5$	$\rho = 1$
SIM + Proposed Approach	5.4 s	5 s	21.4 s
SIM + MNA-based Approach	8.2 s	8 s	24.3 s

[42]. The circuit is composed of multiple nonlinear elements that allow to turn elementary signals (e.g., sinusoids, triangular waves, etc.) into complex waveforms rich in overtones. The circuit parameters are set as follows: $R_1 = 100$ kΩ, $R_2 = 100$ kΩ, $R_3 = 33$ kΩ, $R_4 = 2.7$ kΩ, $R_5 = 27$ kΩ, $R_6 = R_7 = R_8 = R_9 = R_{10} = R_{11} = R_{12} = R_{13} = 15$ kΩ, $R_{14} = 5.6$ kΩ, $R_{15} = 5.6$ kΩ, $R_{16} = 56$ kΩ, $R_{17} = 6.8$ kΩ, $R_{18} = 56$ kΩ, $R_{19} = 470$ Ω, and $R_{20} = 500$ kΩ. Potentiometer P_1 is modeled by means of a time varying resistor $R_{\mathrm{pot}} = \mu P_1$, where $P_1 = 10$ kΩ and $\mu \in (0, 1]$. Also in

This article has been accepted for publication in a future issue of this journal, but has not been fully edited. Content may change prior to final publication. Citation information: DOI 10.1109/TASLP.2021.3120627, IEEE/ACM Transactions on Audio, Speech, and Language Processing

GIAMPICCOLO *et al.*: WAVE DIGITAL MODELING AND IMPLEMENTATION OF NONLINEAR AUDIO CIRCUITS WITH NULLORS   11

$$
\tilde{\mathbf{Q}}_{\mathrm{V}} = \begin{bmatrix} 1 & 0 & 0 & 0 & 0 & 0 & 0 & 0 & 0 & 0 \\ 0 & 0 & 0 & 0 & 0 & 0 & 0 & 0 & 0 & 0 \\ 0 & 0 & 0 & 0 & 0 & 0 & 0 & 0 & 0 & 0 \\ 0 & 0 & 0 & 0 & 0 & 0 & 0 & 0 & 0 & 0 \\ 0 & 1 & 0 & 0 & 0 & 0 & 0 & 0 & 0 & 0 \\ 0 & 0 & 0 & 0 & 0 & 0 & 0 & 0 & 0 & 0 \\ 0 & 0 & 0 & 0 & 0 & 0 & 0 & 0 & 0 & 0 \\ 0 & 0 & 1 & 0 & 0 & 0 & 0 & 0 & 0 & 0 \\ 0 & 0 & 0 & 1 & 0 & 0 & 0 & 0 & 0 & 0 \\ 0 & 0 & 0 & 0 & 1 & 0 & 0 & 0 & 0 & 0 \\ 0 & 0 & 0 & 0 & 0 & 1 & 0 & 0 & 0 & 0 \\ 0 & 0 & 0 & 0 & 0 & 0 & 1 & 0 & 0 & 0 \\ 0 & 0 & 0 & 0 & 0 & 0 & 0 & 1 & 0 & 0 \\ 0 & 0 & 0 & 0 & 0 & 0 & 0 & 0 & 1 & 0 \\ 0 & 0 & 0 & 0 & 0 & 0 & 0 & 0 & 0 & 1 \end{bmatrix}
\qquad
\tilde{\mathbf{Q}}_{\mathrm{I}} = \begin{bmatrix} 1 & 0 & 0 & 0 & 0 & 0 & 0 & 0 & 0 & 0 \\ -1 & 0 & 0 & 0 & 0 & 0 & 0 & 0 & 0 & 0 \\ 0 & 0 & 0 & 0 & 0 & 0 & 0 & 0 & 0 & 0 \\ 0 & 0 & 0 & 0 & 0 & 0 & 0 & 0 & 0 & 0 \\ 0 & -1 & 0 & 0 & 0 & 0 & 0 & 0 & 0 & 0 \\ 0 & 0 & 0 & 0 & 0 & 0 & 0 & 0 & 0 & 0 \\ 0 & 0 & 0 & 0 & 0 & 0 & 0 & 0 & 0 & 0 \\ 0 & 0 & 1 & 0 & 0 & 0 & 0 & 0 & 0 & 0 \\ 0 & 0 & 0 & 1 & 0 & 0 & 0 & 0 & 0 & 0 \\ 0 & 0 & 0 & 0 & 1 & 0 & 0 & 0 & 0 & 0 \\ 0 & 0 & 0 & 0 & 0 & 1 & 0 & 0 & 0 & 0 \\ 0 & 0 & 0 & 0 & 0 & 0 & 1 & 0 & 0 & 0 \\ 0 & 0 & 0 & 0 & 0 & 0 & 0 & 1 & 0 & 0 \\ 0 & 0 & 0 & 0 & 0 & 0 & 0 & 0 & 1 & 0 \\ 0 & 0 & 0 & 0 & 0 & 0 & 0 & 0 & 0 & 1 \end{bmatrix}
$$

Fig. 10. Wave folder: matrices $\tilde{\mathbf{Q}}_{\mathrm{V}}$ and $\tilde{\mathbf{Q}}_{\mathrm{I}}$ required for the formation of $\mathbf{S_{11}}$.

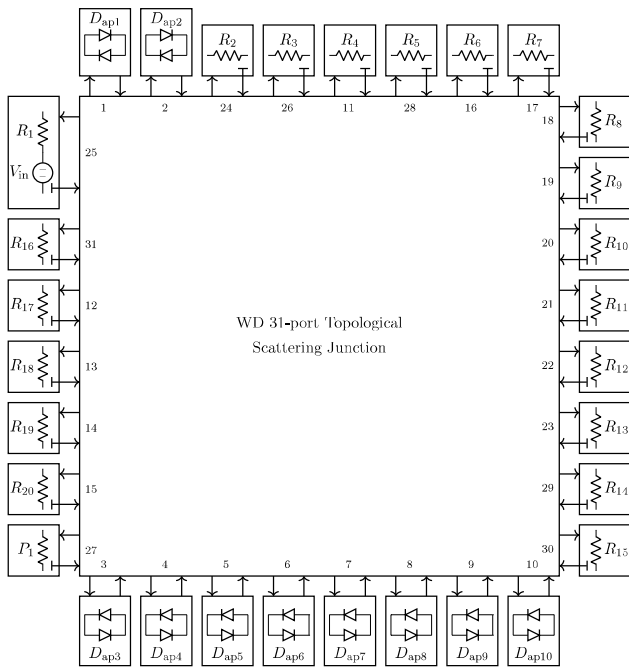

Fig. 11. Wave Digital implementation of the circuit shown in Fig. 8. The T-shaped stubs indicate port adaptation.

Fig. 12. Different plots of the output voltage related to the circuit shown in Fig. 8 obtained tweaking parameter μ (controlling potentiometer P_1), i.e., varying the wave folding. (a) Output voltage with $\mu = 0.25$; (b) output voltage with $\mu = 0.5$; (c) output voltage with $\mu = 1$. The blue curve represents the WD implementation, whereas the dashed red curve the LTspice implementation.

this case, the nonlinear elements of the circuit are 1N4148 diodes, and the parameters of the Shockley model are the same employed in Subsection V-A. The pair of antiparallel diodes is modeled using a single WD nonlinear element, as described in Subsection II-B. The WD realization of the wave folder circuit is shown in Fig. 11. As in the previous example, assuming the opamps to be ideal, it is possible to exploit the method explained in Section III to encompass the nullor-based equivalent models in the WD 31-port topological junction. All the free parameters are set according to SIM "Initialization and Update" stage described in Section IV. As far as the computation of the scattering matrix is concerned, by applying the double-digraph decomposition we obtain a number $t = 15$ of twigs and a number $l = 16$ of links. It follows that (37) is less computationally demanding than (38) and thus a cut-set anal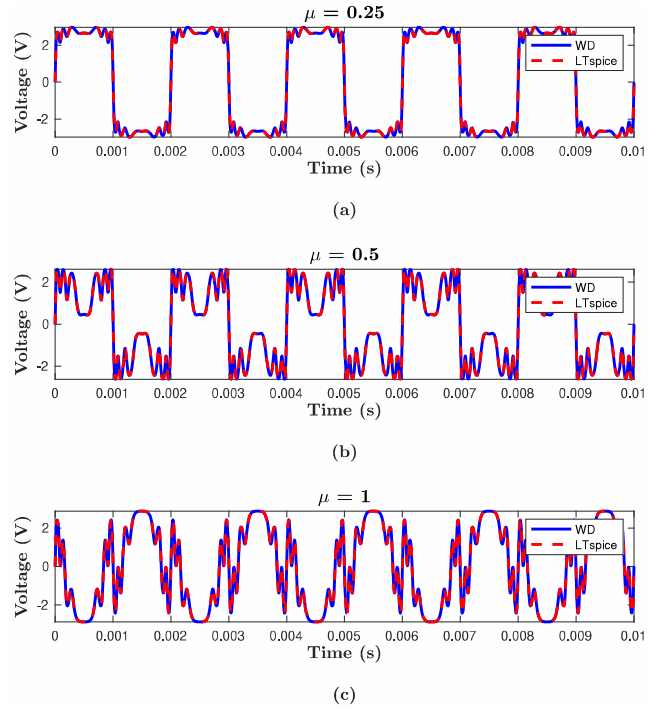ysis is performed. Knowing that the nonlinearities are connected to the first ten ports, submatrix $\mathbf{S_{11}}$ can be assessed employing (60) and considering the matrices shown in Fig. 10. Unlike what we obtained for the precision half-wave rectifier, matrices $\tilde{\mathbf{Q}}_{\mathrm{V}}$ and $\tilde{\mathbf{Q}}_{\mathrm{I}}$ are not equal, and thus $\mathbf{S_{11}}$ will not generally be symmetric for any value of ρ.

We set the the input signal as $V_{\mathrm{in}}[k] = A \sin(2\pi k f_0 / f_{\mathrm{s}})$ where $A = 3$ V, $f_0 = 500$ Hz, and $f_{\mathrm{s}} = 44.1$ kHz. The output voltage of the circuit, instead, is shown in Fig. 12, where it is depicted for three different values of μ, i.e., the parameter modeling potentiometer P_1 and thus controlling the wave folding. The matching between the curves assures the accuracy of the proposed method.

TABLE III

WAVE FOLDER: COMPARISON BETWEEN THE AVERAGE SIMULATION TIME OF SIM COUPLED TO THE PROPOSED APPROACH AND TO THE MNA-BASED APPROACH FOR DIFFERENT VALUES OF ρ.

	$\rho = 0$	$\rho = 0.5$	$\rho = 1$
SIM + Proposed Approach	20.1 s	23.8 s	23.7 s
SIM + MNA-based Approach	32.8 s	37.1 s	36.8 s

As a final test, we consider as input signal $V_{\text{in}}[k]$ a periodic triangular wave with amplitude $A = 3$ V, fundamental frequency $f_0 = 500$ Hz and sampling frequency $f_s = 44.1$ kHz. Table III shows a comparison regarding t_{sim} for 5 s of simulation between SIM coupled to the proposed approach for the computation of the scattering matrix and SIM coupled to the MNA-based approach [17]. The cases of $\rho = 0$, $\rho = 0.5$, and $\rho = 1$ are considered. The results are averaged over 100 identical runs of the two algorithms. Also this example confirms that the double-digraph technique proposed in this manuscript for the formation of the scattering matrix turns out to be more efficient than the state-of-the-art method. Moreover, the advantage is even more remarked than in the previous example, since the size of the matrix to be inverted for the MNA-based approach is 23×23, whereas for the proposed approach is 15×15.

VI. CONCLUSIONS

In this manuscript, we proposed an efficient method for the derivation of scattering matrices of WD junctions absorbing nullors, which are theoretical two-ports useful for modeling several multi-port devices in audio circuits, such as linear opamps. The proposed method is based on a double-digraph decomposition of the reference connection network containing nullors, which is generally nonreciprocal and nonlossless, into a pair of reciprocal and lossless connection networks (the V-network and the I-network). By merging the information of the V-network and the I-network, we then derived two formulas for computing the matrices of the scattering junctions. Such formulas are characterized by a reduced computational cost w.r.t. the state-of-the-art MNA-based method discussed in [17]. The proposed methodology turned out to be particularly useful for the simulation of circuits with multiple nonlinearities through the Scattering Iterative Method (SIM) [9], [13], [16], a fixed-point method that has shown, over the past few years, great performance in emulating audio circuits with multiple nonlinearities, since it requires a frequent update of the scattering matrices of the topological junctions. In fact, in order to emulate nonlinear audio circuits containing active elements, iterative procedure are usually required to break the delay-free-loops formed at the interconnections between WD blocks. In addition, specific criteria of convergence are given for the case of nonreciprocal scattering junctions absorbing nullors.

It is worth noticing that a straightforward extension of the proposed method can be done for the WD realization of topological junctions embedding both nullors and ideal transformers by integrating the approach discussed in [18] with the methodology described in this manuscript.

REFERENCES

[1] V. Välimäki, F. Fontana, J. O. Smith, and U. Zölzer, "Introduction to the special issue on virtual analog audio effects and musical instruments," *IEEE Transactions on Audio, Speech, and Language Processing*, vol. 18, no. 4, pp. 713–714, 2010.

[2] E. Barbour, "Cool sound of tubes," *IEEE Spectrum*, vol. 35, no. 8, pp. 24–35, aug 1998.

[3] A. Wright, E. P. Damskägg, and V. Välimäki, "Real-Time Black-Box Modelling With Recurrent Neural Networks," in *Proceedings of the 22nd International Conference on Digital Audio Effects (DAFx-19)*, sep 2019.

[4] D. Bouvier, T. Hélie, and D. Roze, "Phase-based order separation for Volterra series identification," *International Journal of Control*, vol. 94, no. 8, pp. 2104–2114, aug 2021.

[5] G. Borin, G. De Poli, and D. Rocchesso, "Elimination of delay-free loops in discrete-time models of nonlinear acoustic systems," *IEEE Transactions on Speech and Audio Processing*, vol. 8, no. 5, pp. 597–604, 2000.

[6] A. Falaize and T. Hélie, "Simulation of an analog circuit of a wah pedal: A port-hamiltonian approach," in *Proceedings of the 135th Audio Engineering Society Convention*, Rome, Italy, may 2013, pp. 548–556.

[7] A. Fettweis, "Wave Digital Filters: Theory and Practice," *Proceedings of the IEEE*, vol. 74, no. 2, pp. 270–327, 1986.

[8] P. B. Johns and M. O'Brien, "Use of the Transmission-Line Modelling (t.l.m.) Method to Solve Nonlinear Lumped Networks," *Radio and Electronic Engineer*, vol. 50, no. 1.2, pp. 59–70, 1980.

[9] A. Bernardini, P. Maffezzoni, and A. Sarti, "Linear Multistep Discretization Methods with Variable Step-Size in Nonlinear Wave Digital Structures for Virtual Analog Modeling," *IEEE/ACM Transactions on Audio, Speech, and Language Processing*, vol. 27, no. 11, pp. 1763–1776, 2019.

[10] S. Bilbao, *Wave and Scattering Methods for Numerical Simulation.* Chichester, UK: John Wiley and Sons, Ltd, may 2004.

[11] T. Schwerdtfeger and A. Kummert, "A Multidimensional Approach to Wave Digital Filters with Multiple Nonlinearities," in *Proceedings of the 22nd European Signal Processing Conference (EUSIPCO)*, Lisbon, Portugal, sep 2014, pp. 2405–2409.

[12] M. J. Olsen, K. J. Werner, and J. O. Smith, "Resolving Grouped Nonlinearities in Wave Digital Filters Using Iterative Techniques," in *Proceedings of the 19th International Conference on Digital Audio Effects (DAFx-16)*, Brno, Czech Republic, sep 2016.

[13] A. Bernardini, P. Maffezzoni, L. Daniel, and A. Sarti, "Wave-Based Analysis of Large Nonlinear Photovoltaic Arrays," *IEEE Transactions on Circuits and Systems I: Regular Papers*, vol. 65, no. 4, pp. 1363–1376, 2018.

[14] L. Kolonko, J. Velten, and A. Kummert, "Automatic differentiating wave digital filters with multiple nonlinearities," in *Proceedings of the 28th European Signal Processing Conference (EUSIPCO)*, Amsterdam, Netherlands, jan 2021, pp. 146–150.

[15] R. Giampiccolo, A. Bernardini, G. Gruosso, P. Maffezzoni, and A. Sarti, "Multiphysics Modeling of Audio Circuits with Nonlinear Transformers," *Journal of the Audio Engineering Society*, vol. 69, no. 6, pp. 374–388, jun 2021.

[16] A. Proverbio, A. Bernardini, and A. Sarti, "Toward the Wave Digital Real-Time Emulation of Audio Circuits with Multiple Nonlinearities," in *Proceedings of 28th European Signal Processing Conference (EUSIPCO)*, Amsterdam, The Netherlands, jan 2021, pp. 151–155.

[17] K. J. Werner, A. Bernardini, J. O. Smith, and A. Sarti, "Modeling Circuits with Arbitrary Topologies and Active Linear Multiports Using Wave Digital Filters," *IEEE Transactions on Circuits and Systems I: Regular Papers*, vol. 65, no. 12, pp. 4233–4246, 2018.

[18] A. Bernardini, K. J. Werner, J. O. Smith, and A. Sarti, "Generalized Wave Digital Filter Realizations of Arbitrary Reciprocal Connection Networks," *IEEE Transactions on Circuits and Systems I: Regular Papers*, vol. 66, no. 2, pp. 694–707, 2019.

[19] G. O. Martens and K. Meerkötter, "On N-Port adaptors for Wave Digital Filters with Application to a Bridged-Tee Filter," in *Proceedings of IEEE International Symposium on Circuits and Systems (ISCAS)*, 1976, pp. 514–517.

[20] A. Bernardini, P. Maffezzoni, and A. Sarti, "Vector Wave Digital Filters and Their Application to Circuits With Two-Port Elements," *IEEE Transactions on Circuits and Systems I: Regular Papers*, vol. 68, no. 3, pp. 1269–1282, 2021.

[21] O. Bogason and K. J. Werner, "Modeling circuits with operational transconductance amplifiers using wave digital filters," in *Proceedings of the 20th International Conference on Digital Audio Effects (DAFx-17)*, Edimburgh, UK, sep 2017, pp. 130–137.

This article has been accepted for publication in a future issue of this journal, but has not been fully edited. Content may change prior to final publication. Citation information: DOI 10.1109/TASLP.2021.3120627, IEEE/ACM Transactions on Audio, Speech, and Language Processing

GIAMPICCOLO et al.: WAVE DIGITAL MODELING AND IMPLEMENTATION OF NONLINEAR AUDIO CIRCUITS WITH NULLORS 13

[22] K. J. Werner, W. R. Dunkel, M. Rest, M. J. Olsen, and J. O. Smith, "Wave digital filter modeling of circuits with operational amplifiers," in *Proceedings of the 24th European Signal Processing Conference (EUSIPCO)*, Budapest, Hungary, aug 2016, pp. 1033–1037.

[23] B. Myers and G. Martinelli, "Nullor model of the transistor," *Proceedings of the IEEE*, vol. 53, no. 7, pp. 758–759, 1965.

[24] H. J. Carlin, "Singular network elements," *IEEE Transactions on Circuit Theory*, vol. 11, no. 1, pp. 67–72, 1964.

[25] B. D. Tellegen, "On Nullators and Norators," *IEEE Transactions on Circuit Theory*, vol. 13, no. 4, pp. 466–469, 1966.

[26] A. C. Davies, "The Significance of Nullators, Norators and Nullors in Active-network Theory," *Radio and Electronic Engineer*, vol. 34, no. 5, pp. 259–267, 1967.

[27] A. Bernardini and A. Sarti, "Towards Inverse Virtual Analog Modeling," in *Proceedings of the 22nd International Conference on Digital Audio Effects (DAFx-19)*, Birmingham, UK, sep 2019.

[28] G. Kubin, "Wave Digital Filters: Voltage, Current, or Power Waves?" in *Proceedings of IEEE International Conference on Acoustics, Speech and Signal Processing (ICASSP)*, vol. 10, Tampa, FL, USA, apr 1985, pp. 69–72.

[29] R. C. D. De Paiva, S. D'Angelo, J. Pakarinen, and V. Välimäki, "Emulation of operational amplifiers and diodes in audio distortion circuits," *IEEE Transactions on Circuits and Systems II: Express Briefs*, vol. 59, no. 10, pp. 688–692, oct 2012.

[30] A. Bernardini, K. J. Werner, A. Sarti, and J. O. Smith, "Modeling Nonlinear Wave Digital Elements Using the Lambert Function," *IEEE Transactions on Circuits and Systems I: Regular Papers*, vol. 63, no. 8, pp. 1231–1242, 2016.

[31] D. Albertini, A. Bernardini, and A. Sarti, "Antiderivative Antialiasing Techniques in Nonlinear Wave Digital Structures," *Journal of the Audio Engineering Society*, vol. 69, no. 7/8, pp. 448–464, 2021.

[32] S. D'Angelo, L. Gabrielli, and L. Turchet, "Fast Approximation of the Lambert W Function for Virtual Analog Modelling," in *Proceedings of the 22nd International Conference on Digital Audio Effects (DAFx-19)*, Birmingham, UK, sep 2019, pp. 238–244.

[33] S. Seshu and M. B. Reed, *Linear Graphs and Electrical Networks*. AddisonWesley Publishing Company, Inc. Reading, 1961.

[34] M. Pierzchała and M. Fakhfakh, "Symbolic analysis of nullor-based circuits with the two-graph technique," *Circuits, Systems, and Signal Processing*, 2014.

[35] L. O. Chua, C. Desoer, and E. Kuh, *Linear and Nonlinear Circuits*. McGraw-Hill, 1987.

[36] K. Meerkötter and D. Fränken, "Digital Realization of Connection Networks by Voltage-Wave Two-Port Adaptors," *AEU - International Journal of Electronics and Communications*, vol. 50, no. 6, pp. 362–367, 1996.

[37] J. A. Svoboda, "Unique solvability of RLC nullor networks," *International Journal of Circuit Theory and Applications*, vol. 11, no. 1, pp. 1–6, 1983.

[38] R. P. Sallen and E. L. Key, "A practical method of designing RC active filters," *IRE Transactions on Circuit Theory*, vol. 2, no. 1, pp. 74–85, 2013.

[39] J. Tow, "Active RC Filters—A State-Space Realization," *Proceedings of the IEEE*, vol. 56, no. 6, pp. 1137 – 1139, 1968.

[40] D. Albertini, A. Bernardini, and A. Sarti, "Scattering Iterative Method based on Generalized Wave Variables for the Implementation of Audio Circuits with Multiple One-Port Nonlinearities," in *Proceedings of the 150th Audio Engineering Society Convention*, Online, jun 2021.

[41] A. Bernardini, E. Bozzo, F. Fontana, and A. Sarti, "A Wave Digital Newton-Raphson Method for Virtual Analog Modeling of Audio Circuits with Multiple One-Port Nonlinearities," *IEEE/ACM Transactions on Audio, Speech, and Language Processing*, vol. 29, pp. 2162 – 2173, 2021.

[42] J. Haible, "Wave Multiplier B," 2001. [Online]. Available: http://jhaible.com/legacy/jh_shaper_B.pdf

[43] Mutable Instruments, "Manual and schematic of Kinks module," 2019. [Online]. Available: https://mutable-instruments.net/modules/kinks/

Riccardo Giampiccolo (GSM'20) received both the B.S. and the M.S. degrees in Electronics Engineering from the Politecnico di Milano, Italy, in 2017 and 2020, respectively. He is currently a Ph.D. Candidate in Information Technology at the Dipartimento di Elettronica, Informazione e Bioingegneria of the Politecnico di Milano, Italy. His main research interests are related to signal processing methodologies for small-size transducers in consumer electronics.

Mauro Giuseppe de Bari obtained both the B.S. degree in Computer Science and Engineering and the M.S. degree (cum laude) in Telecommunications Engineering - Musical Acoustics from the Politecnico di Milano, Italy, in 2017 and 2020, respectively. He is currently working as DSP engineer on digital filters and VA algorithms at Arturia.

Alberto Bernardini (S'16-M'19) received the B.S. degree from the University of Bologna, Italy, and M.S. degree (cum laude) from the Politecnico di Milano, Italy, both in computer engineering, in 2012 and 2015, respectively. In 2019, he received his Ph.D. degree (cum laude) in information engineering from Politecnico di Milano, Italy, where he is currently a Postdoctoral Researcher. His main research interests are audio signal processing and modeling of nonlinear systems. He authored more than 20 publications in international journals and proceedings of international conferences. He is also the first author of an international patent.

Augusto Sarti (M'04-SM'13) received his Ph.D. in Information Engineering from the University of Padova, Italy, in 1993, with a joint graduate program with the University of California, Berkeley. In 1993, he joined the Politecnico di Milano (PoliMI), Italy, where he is currently a Full Professor. From 2013 to 2017 he held a professorship at the University of California, Davis. At PoliMI he currently coordinates the research activities of the Musical Acoustics Lab and the Sound and Music Computing Lab, and the M.Sci. program in "Music and Acoustic Engineering". He has coauthored well over 300 scientific publications on international journals and congresses and numerous patents in the multimedia signal processing area. His current research interests are in the area of audio and acoustic signal processing, with particular focus on audio and acoustic signal processing; music information retrieval; and musical acoustics. He served two terms with the IEEE Technical Committee on Audio and Acoustics Signal Processing. He also served as Associate Editor of IEEE/ACM Tr. on Audio Speech and Language Processing, and as Senior Area Editor of IEEE Signal Processing Letters. He is currently serving in the EURASIP board of directors.